Novel Porous Boron Nitride Nanosheet with Carbon Doping: Potential Metal-Free Photocatalyst for Visible-Light-Driven Overall Water Splitting

Qiang Wan, Fenfei Wei, Zuju Ma, Masakazu Anpo, and Sen Lin**

The band gap of hexagonal boron nitride (*h*-BN) is far too wide for efficiently utilizing visible light, limiting its application in photocatalysis. The present study employs first principles calculations to demonstrate that the band gap energies of porous *h*-BN (*p*-BN) can be tuned by carbon doping to levels appropriate for the absorption of visible-light, and that the conduction band and valence band match well with the potentials of both hydrogen and oxygen evolution reactions. Importantly, a strategy of carbon doping to improve the energy level of valence band maximum is also proposed. Moreover, the carbon-doped *p*-BN exhibits good separation between photogenerated electrons/holes and structural stability at high temperatures. The DFT results help the design of high-performance two-dimensional photocatalysts that avoid the use of metals.

1. Introduction

The extraordinary electronic properties of single-atomic-layer graphene sheets successfully isolated by Novoselov et al.[1] has led to the wide development of two-dimensional (2D) nanomaterials, such as hexagonal boron nitride (*h*-BN),[2] BCN,[3] and graphitic carbon nitride (g-C_3N_4),[4] in the past few years. These represent very promising materials due to their peculiar physical/chemical properties, as well as for their potential applications in diverse areas such as electronics, optoelectronics, energy storage and conversion, and hybrid materials.[5] In particular, a number of 2D materials are suitable as photocatalysts owing to their appropriate band structures.[6] For example, Wang et al.[4a] had reported that g-C_3N_4, with a band gap of 2.70 eV, could be used to photocatalyze hydrogen and oxygen from water under visible light irradiation. This opens an entirely new direction for developing metal-free photocatalysts for overall water splitting.

Among the several 2D materials available, *h*-BN, an analogue of graphene, has attracted tremendous interest recently due to its electronic properties that are distinct from those of graphene and its superior mechanical, thermal, and chemical stabilities. However, *h*-BN is an insulator owing to its wide band gap of about 5.56 eV.[2a,7] Unfortunately, the standard band gap of *h*-BN is far too wide for efficiently utilizing visible light, and thus limits its application in photocatalysis.[8] Nonetheless, recent experimental and theoretical studies have demonstrated that the band structure of *h*-BN can be successfully modified by various physical and chemical methods.[3c,9] For example, Li et al.[10] suggested based on theoretical analysis that semi-hydrogenated *h*-BN was a potential photocatalyst for water splitting under visible light irradiation owing to a band gap of around 2.24 eV with advantageous conduction band (CB) and valence band (VB) energies ensuring that the redox potentials of water splitting are both located between the band gap. However, semi-hydrogenated *h*-BN permits the hydrogen evolution reaction (HER) because the reduction level is quite close to the position of CB, indicates a relatively weak driving force. From an experimental perspective,[3c] it has been suggested that the control of the carbon concentration in C-doped *h*-BN to form various quantities of boron carbon nitrides could provide an additional means of tuning the band structures of *h*-BN. Huang et al.[3c] experimentally demonstrated that introducing C atoms to *h*-BN (BCN) can efficiently narrow the band gap, which is confirmed by our DFT calculations. Although the photocatalytic generation of hydrogen from water under visible light irradiation can be realized using BCN without using noble metals as a cocatalyst, the efficiency of the oxygen evolution reaction (OER) is still quite low due to the high energy level of the top of the VB. Similar results have been found for g-C_3N_4.[4a,11] The inability of configurations of *h*-BN with extensive carbon doping modes, including different carbon contents and clustering, to provide a suitable VB for the OER has also been demonstrated in a theoretical study.[8a] Therefore, developing C-doped *h*-BN configurations with the CB

Q. Wan, F. Wei, Prof. M. Anpo, Prof. S. Lin
State Key Laboratory of Photocatalysis on Energy and Environment
College of Chemistry
Fuzhou University
Fuzhou 350002, China
E-mail: slin@fzu.edu.cn
Prof. Z. Ma
School of Materials Science and Engineering
Anhui University of Technology
Maanshan 243002, China
E-mail: zjma@outlook.com
Prof. M. Anpo
Department of Applied Chemistry
Graduate School of Engineering
Osaka Prefecture University
Sakai, Osaka 599-8531, Japan

The ORCID identification number(s) for the author(s) of this article can be found under https://doi.org/10.1002/adts.201800174

DOI: 10.1002/adts.201800174

and VB straddling both the OER and HER levels remains a substantial challenge.

Previous theoretical studies predicted that creating a porous structure in *h*-BN could decrease its bandgap but with far less knowledge about the photocatalysis.[3c,12] On the other hand, the porous *h*-BN has attracted more and more attention from experiments.[13] For example, Gautam et al. had reported a carbon-doped porous *h*-BN which was successfully been synthesized using very simple solid state rout and exhibited excellent mechanical properties.[13a] In another study by Xiong and coworkers, a novel carbon-doped porous boron nitride had been prepared with the carbon source via calcination under N_2 atmosphere.[13b] This metal-free porous materials display excellent performance of dibenzothiophene adsorption, which is attributed to the exposed atoms along the edges of the pores. Very recently, Wang et al. showed that the band gap of the as-prepared porous BCN nanosheet ranges from 5.5 to 1.0 eV.[13c] The porous BN (*p*-BN) nanosheets exhibit highly specific surface areas and show superior capacitive properties when being applied in supercapacitors. Obviously, *p*-BN has fewer atoms in an equal surface area and the electronic structures are more sensitive to carbon doping when compared to *h*-BN.

In light of the above discussion, the present work focuses on the band gap engineering of *p*-BN via carbon doping to develop a metal-free 2D photocatalyst for catalyzing both the HER and OER, and that effectively separates the photogenerated electrons and holes spatially to limit recombination. To this end, we apply materials modeling at an atomic scale from first principles for conducting electronic structure calculations. To investigate the effect of carbon doping on the band gap, unit *p*-BN structures doped with different numbers of C atoms to model C concentrations of 16.67, 33.3, and 50.0 at%, respectively. The band structures as well as the optical properties of these systems are also investigated. Finally, the dynamic stability of the various systems was evaluated, and their thermal stabilities at elevated temperature were also systematically investigated via quantum-mechanical molecular dynamics (MD) simulations to obtain a good indication of their structural stability. The results obtained from this study might provide some useful insights for designing metal-free 2D photocatalysts for overall water splitting providing stoichiometric proportions of H_2 and O_2.

2. Experimental Section

All calculations were performed using the Vienna Ab Initio Simulation Package (VASP) based on plane-wave basis sets.[14] Projector augmented wave (PAW) potentials were employed for modeling electron-ion interactions,[15] with a plane-wave energy cutoff set to 500 eV. The generalized gradient approximation (GGA) with the Perdew-Burke-Ernzerhof (PBE) functional was adopted for structural optimization.[3c,16] To avoid the well-known underestimation of the semiconductor band gap associated with calculations based on the pure density functional theory (DFT) method,[17] the Heyd-Scuseria-Ernzerhof (HSE06) screened hybrid density functional method was employed to obtain the electronic structures, density of states, and optical absorption coefficients.[18] Electronic states were occupied with Gaussian smearing method, with a smearing width of 0.1 eV for band structure calculation, the total number of valence electrons is 48 for *p*-BN and configurations a–l, in which the systems keep electrical neutral. The convergence settings of energy and force were 0.01 eV $Å^{-1}$ and 10^{-4} eV, respectively.

The present work considered only models composed of a single layer of BN situated in the *x*-*y* plane. To remove spurious interactions between periodic structures in the supercell models along the *z* direction, a vacuum space of 14 Å was adopted. To establish the *p*-BN model, we began with a unit cell of pristine *h*-BN, and optimized the structure. The lattice parameter and B—N bond length of *h*-BN after optimization were 2.50 and 1.42 Å, respectively, which are in good agreement with experimental data.[2b,19] We then introduced BN hexagonal vacancies (black balls in **Figure 1**) into a (3 × 3) supercell (9 B and 9 N) of pristine *h*-BN to construct a *p*-BN. The structural optimized of this configuration with vacancies leads to a significant reconstruction. As shown in Figure 1, the new structure, namely *p*-BN, is quite different from the initial six-ring structure. The *p*-BN unit cell (1 × 1) contains a large central porous ring with 12 atoms (6 B and 6 N) and the calculated lattice parameter is 6.83 Å, which is consistent with the previous reports.[20] Supercells comprising n × n unit cells were employed in the electronic structure, dynamic stability, and thermal stability calculations. For the electronic structure calculations, $n = 1$ was employed, while $n = 3$ was used in phonon spectra calculations based on density functional perturbation theory for evaluating dynamic stability,[19b,21] and supercells with $n = 2$ were employed in Born–Oppenheimer MD (BOMD) simulations conducted at the DFT level using an *NVT* ensemble with 1 fs time steps for thermal stability testing. For thermal stability testing, we adopted the structures obtained from structural relaxation at 0 K as the initial structures, and conducted the BOMD simulations at different temperatures from 300 to 1700 K for a simulated time duration of 5 ps. Thermal stability was determined according to the maximum temperature a given structure was able to sustain without a single bond breaking. The k-points were set to be 9 × 9 × 1 for structure optimization and electronic structure calculations, while 3 × 3 × 1 for stability test. In the electronic structure calculations, we determined the positions of CB minimum (CBM) and VB maximum (VBM) for different materials by setting the vacuum level to zero. The vacuum level was defined by the potential far away from 2D surface and obtained from calculated electrostatic potential.[22] For investigating the effect of carbon doping on the band structure of *p*-BN, we obtained the 12 configurations of C-doped *p*-BN shown in **Figure 2**a–l with varying C concentrations by replacing B and N atoms with C atoms (the total number of electrons remains the same). Figure 2a–c represent a C concentration of 16.67 at% with cluster sizes with 1 or 2 C atoms, Figure 2d–i represent a C concentration of 33.3 at% with cluster sizes with 2 or 4 C atoms, and Figure 2j–l represent a C concentration of 50.0 at% with cluster sizes of with 2 or 6 C atoms. In these structures, the B—N, B—C, N—C, and C—C bond lengths were calculated to be 1.41/1.46, 1.41, 1.41, and 1.46/1.41 Å, respectively. For replacing B/N pairs with carbon atoms (for example, replacing one B atom and one N atom with two carbon atoms), the total number of electrons for the systems is not changed after substitution since C has one more electron than B and one less electron than N. It should be also noted that all the models with carbon doping are electrically neutral.

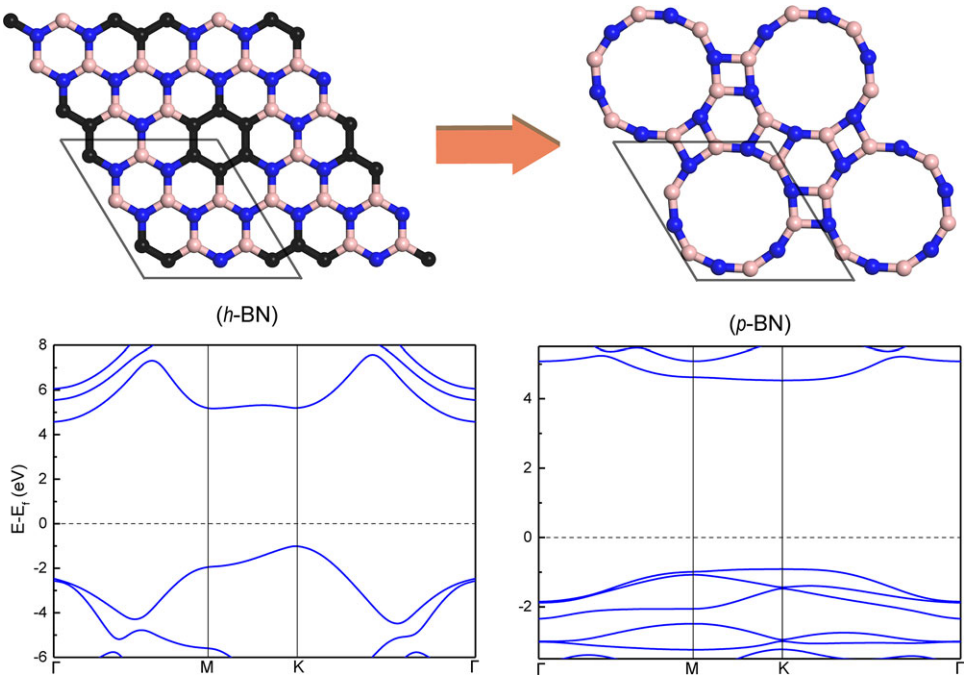

Figure 1. Optimized structures (top view) and band structures of *h*-BN and *p*-BN. The pink, blue, and black balls represent B, N, and atomic vacancies, respectively.

3. Results and Discussion

3.1. Band Structures

The obtained band structures for *h*-BN and pure *p*-BN are shown in Figure 1, the band gap of *h*-BN is computed to be 5.55 eV, very close to the experimental values of 5.56 eV.[2a] For *p*-BN, the band gap of 5.44 eV is still too large for interaction with visible light. **Figure 3** shows the calculated band structures of the C-doped *p*-BN configurations given in Figure 2. The calculated band gaps are summarized in **Table 1** and the total energies are listed in Table S1, Supporting Information. For the C concentration of 16.67%, configuration b possesses the lowest energy. For configurations with C concentration of 33.33%, the energies decrease in the order of g > d > e > f > h > i. For the configurations with C concentration equal to 50.00%, configuration l has the lowest energy. Interestingly, as shown in Figure 2, we can see carbon chains (C—C, C—C—C—C and C—C—C—C—C—C) form in the configurations of b, i, and l which have the lowest energy. For the configurations with the same carbon concentration, it can be assumed that the ones which have lower energies might be more facile to be synthesized in experiment.

For an efficient photocatalyst operable in the visible portion of the solar spectrum, the band gap should be smaller than 3.20 eV. As shown in Table 1, the band gaps of C-doped *p*-BN vary from 1.55 to 3.83 eV. The configurations a, b, and c all have band gaps greater than 3.20 eV, while all other configurations possess band gaps less than 3.20 eV, and therefore may be appropriate for driving the overall water splitting process utilizing the visible portion of the solar spectrum. In addition, we note from Figure 3 that configurations a, d, and i display indirect band gaps, as indicated by CBM values located between the Γ and K points while the corresponding VBM values are located at different positions. All other configurations have direct band gaps, which is beneficial for the utilization of solar energy.

When two C atoms were introduced, the band gaps of configurations of a, b, and c were calculated to be 3.21, 3.83, and 3.23 eV, respectively. In general, the doping of 4 C atoms into *p*-BN (d–i) significantly reduce the band gap from 5.44 to 2.24–2.77 eV. Meanwhile doping with 6 C atoms provided the greatest reduction in the band gap, with the value significantly reduced to 1.55–2.20 eV. **Figure 4**a presents the correlation between the C content and the band gap. It can be clearly seen from the figure that the band gap generally decreases with increasing C content. Moreover, the results of Figure 4b indicate that the VBM generally increases with an increasing number of C—C bonds (n_{C-C}), which reflects the effect of C clustering. Accordingly, the VBM values of the 12 C-doped *p*-BN configurations become generally more positive with an increasing number of C—C bonds. The reason might be that as the VBM of *p*-BN containing the mixing of 2*p* orbitals of C and N would be shifted upward since the C 2*p* orbitals energy is 1.90 eV higher than the N 2*p* orbital energy,[23] and the interaction between C atoms increases the bandwidth of donor states, resulting in the elevation of VB.[24]

To understand the band structure characteristics of C-doped *p*-BN, we analyze the total density of states (TDOS), local density of states (LDOS), and charge distributions of the CB and VB for configurations c, f, h, and l with respective C cluster sizes of 1, 2, 4, and 6, and the results are presented in **Figure 5**a–d, respectively.[25] The TDOS and LDOS for the other configurations are displayed in Figure S1, Supporting Information. Here, the electronic density of states (DOS) are given on the left in the figures, and include the TDOS (top), LDOS (2s orbital; middle), and the LDOS (2p orbital; bottom), and the charge density plots,

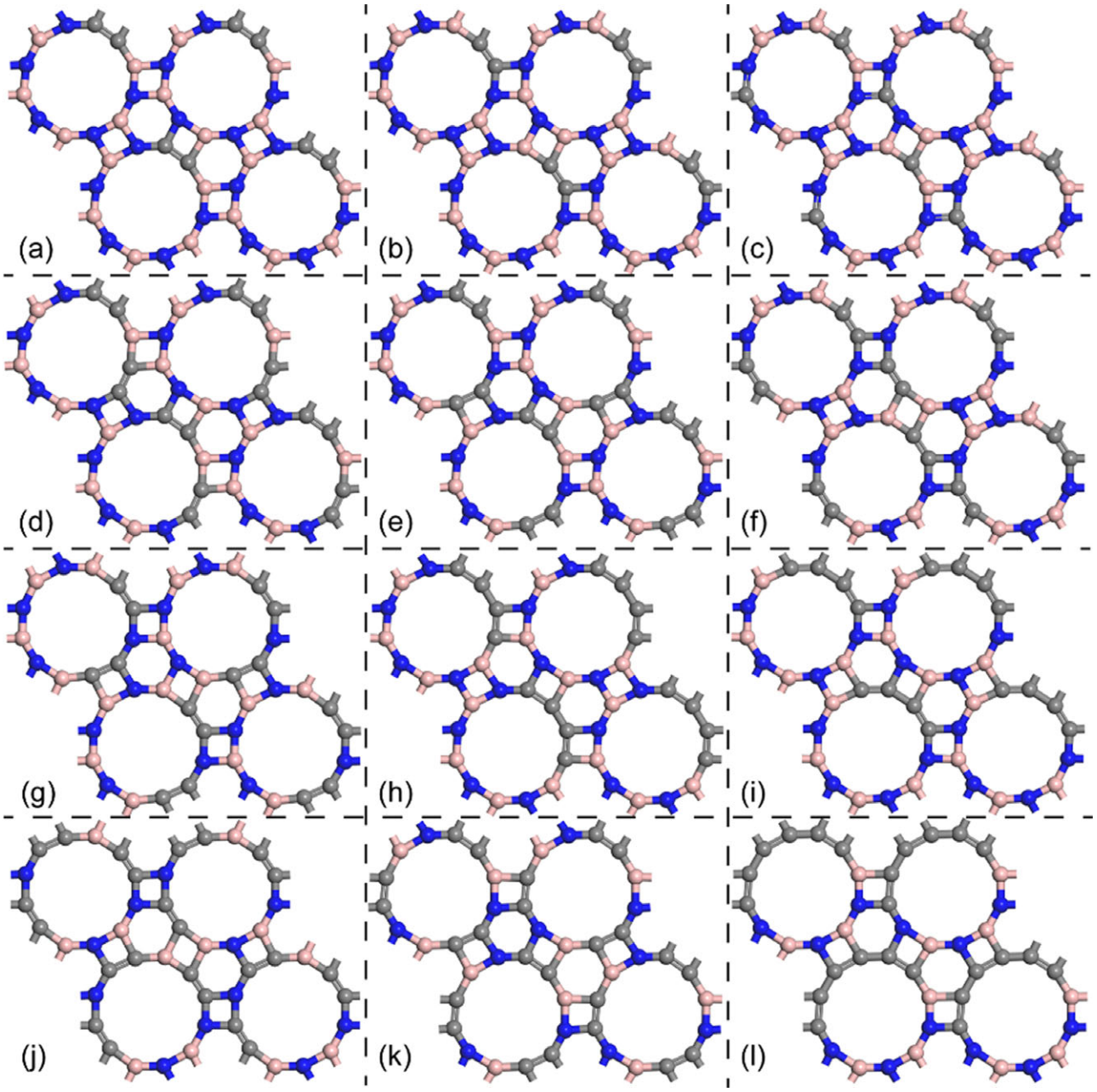

Figure 2. Top views for optimized structures of C-doped *p*-BN with different C concentrations—a–c): 16.67 at%; d–i): 33.33 at%; j–l): 50 at%—and C cluster sizes. The grey, pink, and blue balls represent C, B, and N atoms, respectively.

which are overlaid on the atomic structure of each configuration, are given on the right in the figures for the CB (top) and the VB (bottom). We see from Figure 5 that the 2*s* orbitals of C, N, and B atoms make almost no contribution to the VBM and CBM of C-doped *p*-BN. As the C 2p orbitals energy is 1.90 eV higher than the N 2*p* orbital energy,[23] the VBM contains the mixing of 2*p* orbitals of C and N and shifts upward by 0.71–1.7 eV (Table 1). Meanwhile, we found the CBM of C-doped *p*-BN is mainly dominated by the 2*p* orbitals of B and C atoms. Upon C substitution on B, donor levels are created near the band gap and lower down the CBM by 2.35 eV (Table 1). Interestingly, the defect levels of C atoms are resonant with the VBM and CBM of pure *p*-BN. The 2*p* orbitals of C are close to that of N 2*p* and B 2*p*. No partial occupied/unoccupied states are formed in the forbidden gap, generating clean narrow band gap after doping C atoms. This can inhibit the formation of recombination center and increase the photogenerated current. Furthermore, the partial (band decomposed) charge density plots corresponding to the VBM and CBM for configurations c, f, h, and l (Figure 5) also demonstrate good separation between the probability distributions of the VB and CB. This is important, because the recombination of photoexcited electrons and holes is well

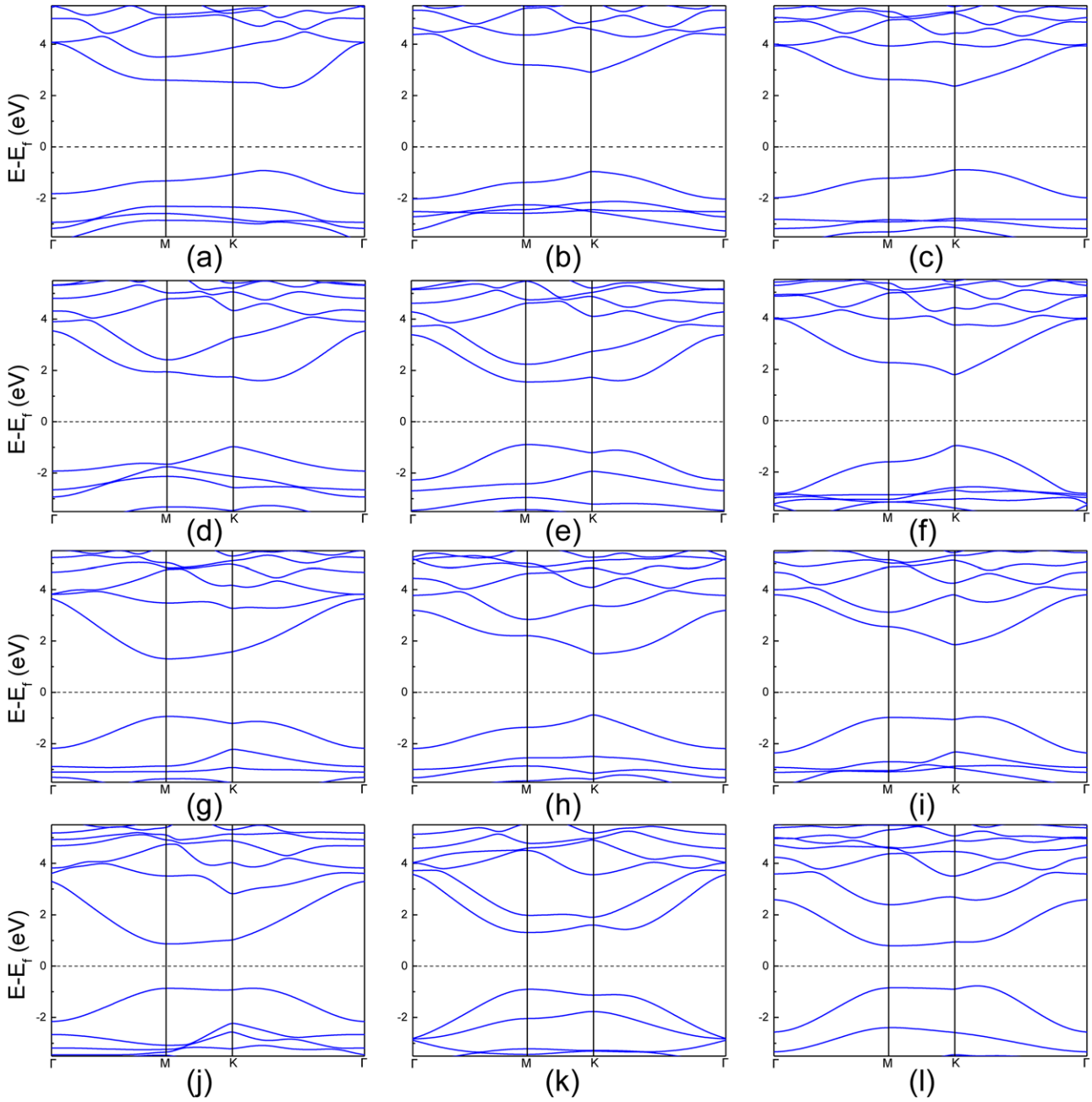

Figure 3. Band structures of the 12 C-doped *p*-BN configurations shown in Figure 2. The Fermi energy is set to 0 eV.

known to be factor that significantly reduces the photocatalytic activity of photocatalysts, and is one of the key factors affecting the performance of photocatalysts employed in water splitting. Therefore, the C-doped *p*-BN configurations discussed here indicate good potential photocatalysts for water splitting.

To explain the mechanism of how the doping of carbon atoms decreases the bandgap of *p*-BN, we investigate the electronic structures of *p*-BN doped with single carbon atom, in which a B atom or a N atom is replaced, respectively. It is seen from Figure S2, Supporting Information that the doping of C atom indeed leads to the decrease of bandgap of *p*-BN. The reason is that when a B atom is replaced by a C atom, an extra state (in red) is created under CBM, while a N atom is substituted by a C atom, one more state (in red) is generated above VBM. In general, when C as the *p*-type dopant is adopted to replace N, acceptor states will be induced above VBM of *p*-BN. When C as the *n*-type dopant is used to substitute B in *p*-BN, donor levels will be created near the CBM.[26] As the C concentration is increased, the acceptor/donor states would interact and extend into the band gap, thus narrowing the band gap of *p*-BN. From the charge distribution of CBM and VBM corresponding to C atom doping in the B and N position in *p*-BN, respectively (Figure S3, Supporting Information), it

Table 1. Calculated band gaps (E_g), valence band maximum (VBM) values, and conduction band minimum (CBM) values of *p*-BN with different C concentrations, and cluster sizes with different numbers of C atoms (unit: eV). The vacuum level was set to 0 eV. The corresponding band structures are shown in Figure 3.

Structure	E_g	CBM	VBM	C at%	Size
p-BN	5.44	−1.47	−6.91	0.00	0
a	3.21	−2.67	−5.88	16.67	2
b	3.83	−2.37	−6.20	16.67	2
c	3.23	−2.51	−5.73	16.67	1
d	2.55	−3.19	−5.73	33.33	2
e	2.43	−3.04	−5.48	33.33	2
f	2.68	−3.09	−5.78	33.33	2
g	2.24	−3.37	−5.60	33.33	2
h	2.33	−3.17	−5.50	33.33	4
i	2.77	−3.03	−5.80	33.33	4
j	1.72	−3.82	−5.53	50.00	2
k	2.20	−3.25	−5.45	50.00	2
l	1.55	−3.66	−5.21	50.00	6

is clearly that this additional state is mainly contributed from the C atom.

3.2. Optical Properties

In addition to an appropriate band gap and suitable band alignment, potential photocatalytic materials must absorb a significant fraction of the incoming light. To examine this factor, the linear optical properties of the modeled 2D C-doped *p*-BN materials were calculated based on the frequency-dependent complex dielectric function using the HSE06 method.[27] The optical absorption spectra are obtained from absorption coefficients evaluated at varying light angular frequencies ω, which can be given by the following equation:

$$\alpha(\omega)=\sqrt{2}\omega\cdot\sqrt{-\varepsilon_1(\omega)+\sqrt{\varepsilon_1^2(\omega)+\varepsilon_2^2(\omega)}} \quad (1)$$

where ε_1 and ε_2 are the real and imaginary parts of the dielectric function, respectively. **Figure 6** shows the absorption spectra of *h*-BN, *p*-BN, and the C-doped *p*-BN configurations c, e, and j, which have moderate band gaps and C contents of 16.67, 33.33, and 50.0 at%, respectively, adsorption spectra for other structures are listed in Figure S4, Supporting Information. We note that *p*-BN has an obviously enhanced optical absorption compared with that of *h*-BN. However, the absorption still remains in the UV region. Nevertheless, after carbon doping, strong absorption is obtained in the visible region, indicating the important role that C doping plays in the utilization of solar energy. Furthermore, we also find that the absorption spectra shift to longer wavelengths (lower photon energy) with increasing C content, which is consistent with the trend associated with the band gap energies of the configurations.

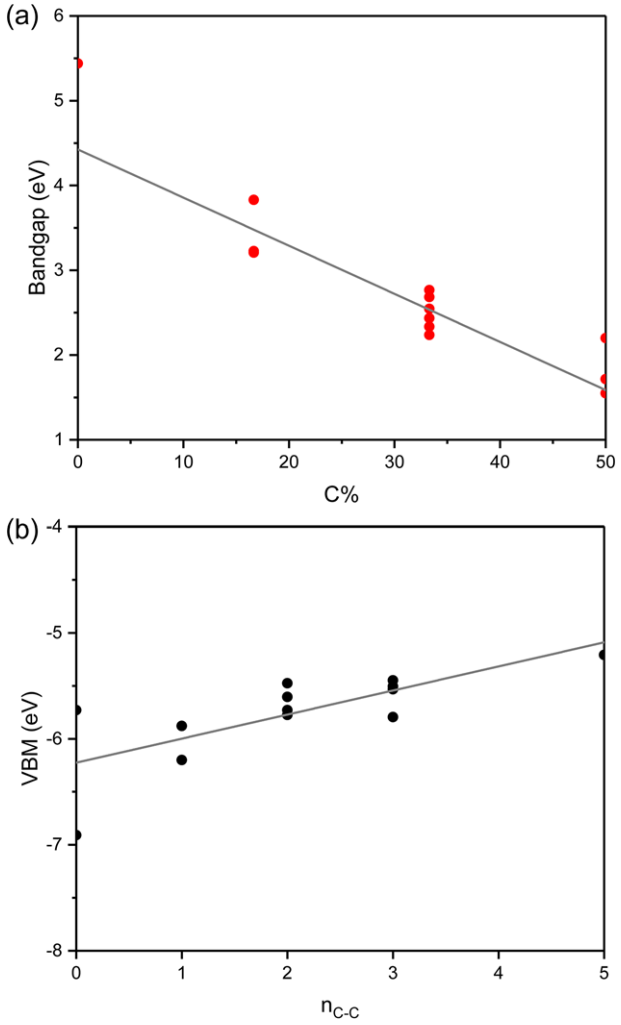

Figure 4. a) Band gaps of the 12 C-doped *p*-BN configurations shown in Figure 2 plotted with respect to the corresponding C contents, and b) the correlation between the numbers of C—C bonds (n_{C-C}) and the valence band maximum (VBM) values of the C-doped *p*-BN configurations.

3.3. Potential for Applications in Water Splitting

As discussed, the overall reaction for water splitting can be divided into the OER and HER half reactions. At pH = 0, the standard reduction potential of H^+/H_2 (HER) is −4.44 eV and the standard oxidation potential of O_2/H_2O (OER) is −5.67 eV, where both of the values are given relative to the vacuum level.[28] These potentials are presented in **Figure 7** along with the CBM and VBM of *h*-BN, pristine *p*-BN, and the 12 C-doped *p*-BN configurations.

The results in Figure 7 indicate that the CBM of all structures considered are more positive than the standard reduction potential of H^+/H_2, indicating that all possess the ability to photocatalyze the hydrogen reduction of water splitting. And for the OER, another half reaction, the VBM values become generally more positive with an increasing C—C bonds (Figure 4b) and lead to the narrower band gaps, but VBM values of some configurations are too positive to drive the OER effectively. At pH = 0, the VBM

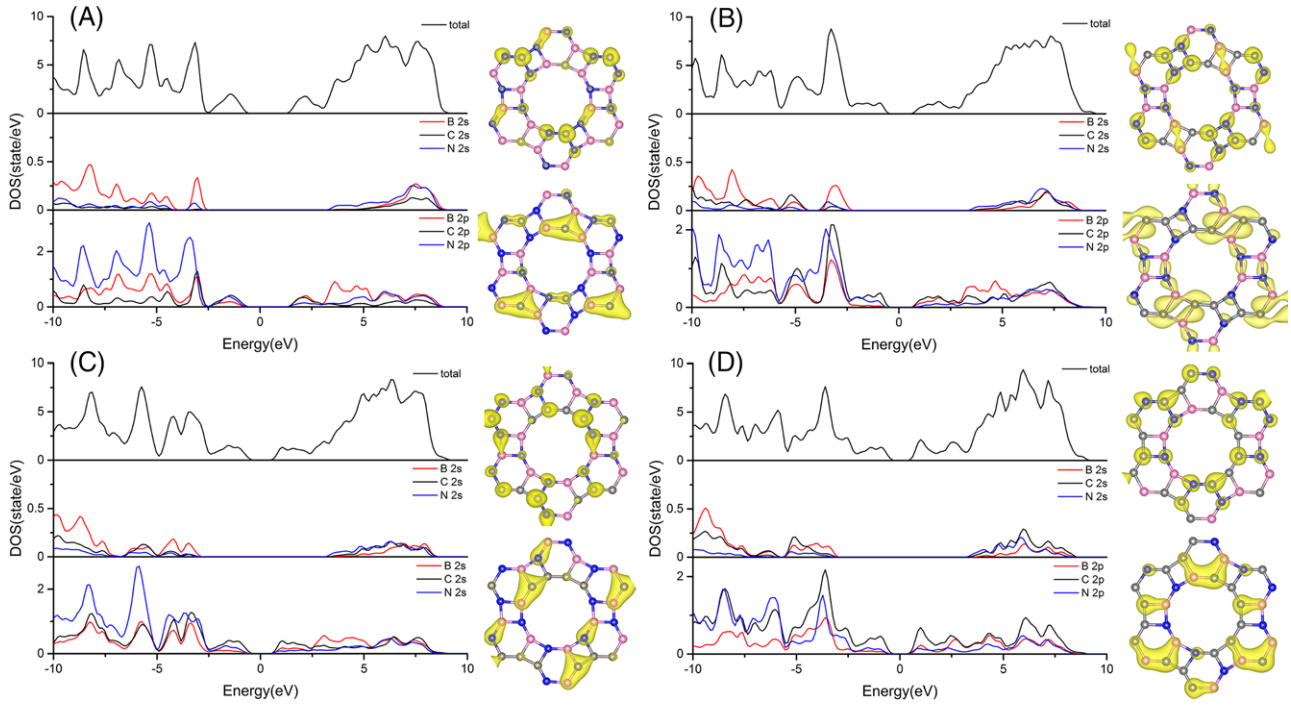

Figure 5. Electronic density of states (DOS) (left), which includes the total DOS (top), the local DOS (2s orbital; middle), and the local DOS (2p orbital; bottom), and charge density plots (right) of the conduction band (CB; top) and the valence band (VB; bottom) for configurations c (A), f (B), h (C), and l (D). The Fermi level is set to zero. The grey, pink, and blue balls represent C, B, and N atoms, respectively.

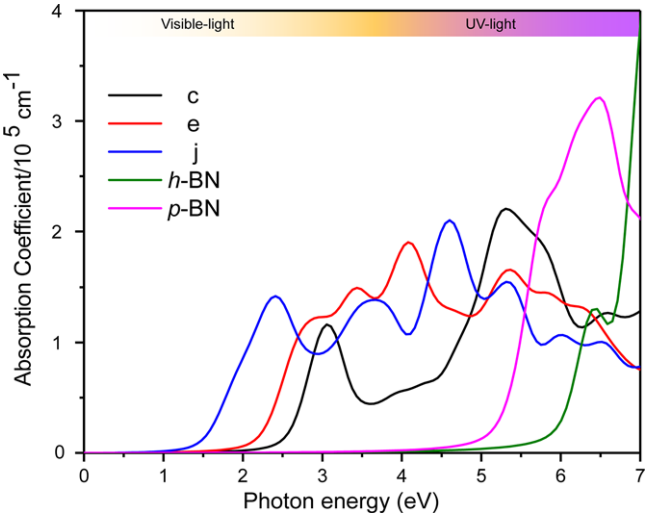

Figure 6. Optical absorption spectra of *h*-BN, pristine *p*-BN, and C-doped *p*-BN configurations c, e, and j.

values of configurations d, f, and i match with the standard potential of the OER. While configurations e, g, h, j, k, and l have more positive VBM values that are not energetically feasible for driving the OER, and fortunately, these structures can play a role in photocatalytic water splitting via serving as a cathode in heterojunction photocatalyst or adding a sacrificial agent. It should be noted that, although the VBM of configuration d, f, and i is more negative than the OER level, its value is quite close to the standard potential of the OER, and can be expected to lack sufficient driving force to ensure an efficient reaction process. This condition is also found for 2D *g*-C_3N_4 photocatalysts.[11]

3.4. Dynamic Stability

The phonon spectra along the high-symmetry points in Brillouin zone were calculated to evaluate the dynamic stability of pristine *p*-BN and the C-doped *p*-BN configurations. The phonon spectra for only pristine *p*-BN, and configurations b, g, and l, are shown in **Figure 8**, which can represent the dynamic stability of C doped *p*-BN with various concentrations, the results for other configurations were given in Figure S5, Supporting Information. As observed in the figure, the phonon dispersions of these configurations are all positive, and no imaginary phonon modes are observed, implying that they are dynamically stable.

3.5. Thermal Stability

The thermal stabilities of *h*-BN, *p*-BN, and configurations b, g, k, and l were evaluated by BOMD simulations in the temperature range from 300 to 1700 K, and the results are shown in **Figure 9**, results for other configurations were shown in Figure S6, Supporting Information. Here, representative top and side views of the structures of the material systems obtained after a simulation time duration of 5 ps are presented at their given maximum sustainable temperatures. While these figures provide little information regarding thermal stability directly, they do provide some measure of the structural deformations sustained

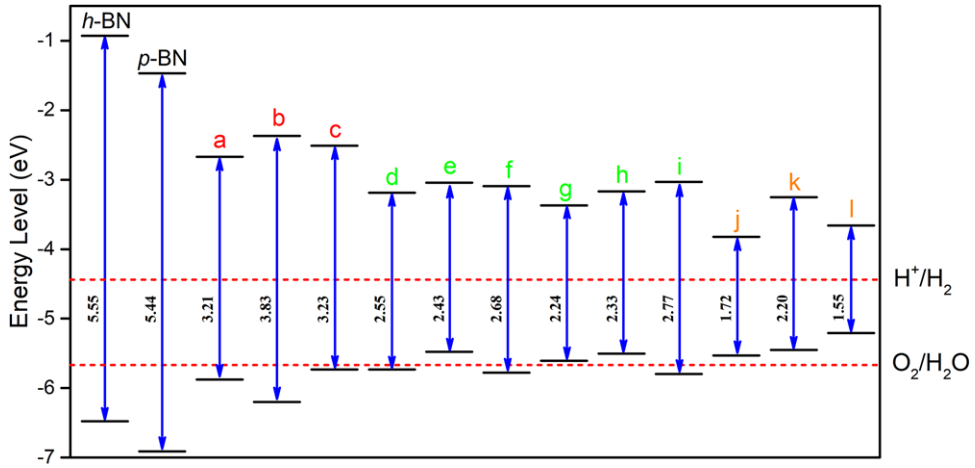

Figure 7. The CBM and VBM of *h*-BN, pristine *p*-BN, and the 12 C-doped *p*-BN configurations. Included are the standard reduction potential of H^+/H_2 (−4.44 eV) and the standard oxidation potential of O_2/H_2O (−5.67 eV) at pH = 0 (relative to the vacuum level).

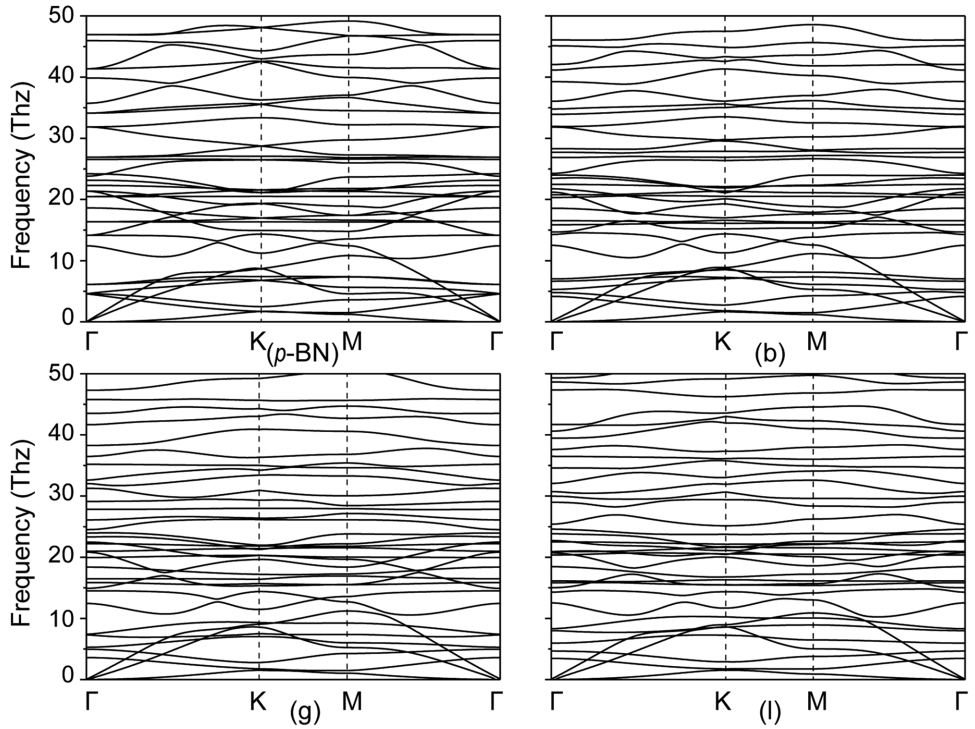

Figure 8. Phonon spectra of pristine *p*-BN, and configurations of b, g, and l.

by the systems at the temperatures given. We note that each of these 2D structures sustains considerable deformation along the *x*-*y* plane. While *h*-BN and *p*-BN remain stable at high temperatures of 1700 and 1500 K, respectively, carbon doping into the *p*-BN lattice substantially decrease the thermal stability of the C-doped *p*-BN configurations, where maximum sustainable temperatures of 1300, 1100, 1100, and 500 K are obtained for configurations b, g, k, and l, respectively. Beyond the maximum temperatures, some chemical bonds of C-doped *p*-BN are broken. In addition, we note that, while both configurations k and l have identical C contents of 50 at%, the more greatly dispersed C atoms in configuration k lead to a much higher maximum sustainable temperature. This is readily understood because graphene, which has a similar structure as that of *h*-BN, but which is composed of carbon atoms, is less stable than *h*-BN at high temperatures.[29]

In general, the bond parameters of the deformed structures obtained by *NVT* simulations at elevated temperatures are very close to those of the initial structures at 0 K. The results certainly indicate that the C-doped *p*-BN configurations considered herein

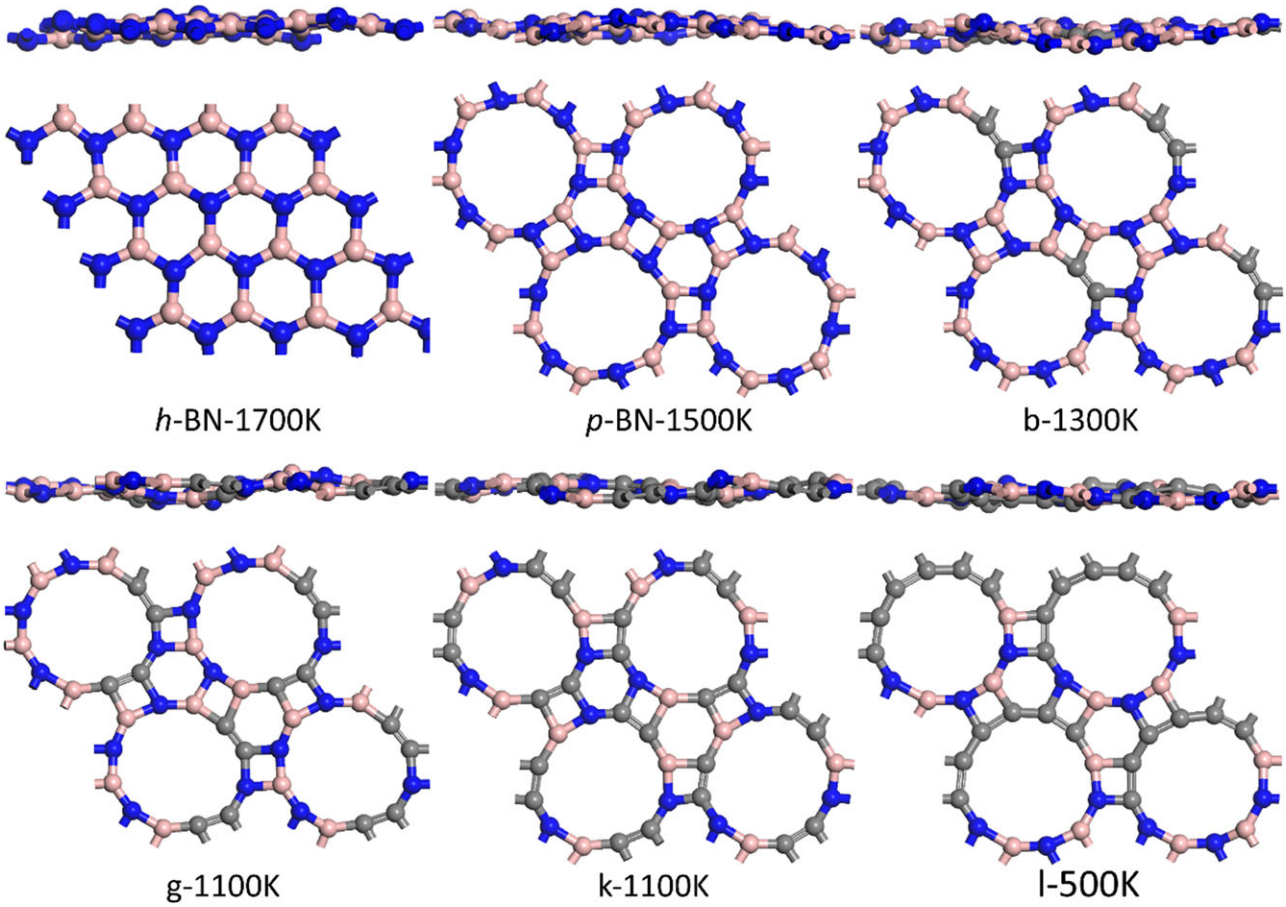

Figure 9. Top and side views of representative structures of *h*-BN, *p*-BN, and configurations b, g, k, and l obtained after conducting Born–Oppenheimer molecular dynamic (BOMD) simulations for 5 ps. The temperatures cited represent the maximum temperature a given structure was able to sustain without a single bond breaking.

are thermally stable at temperatures considerably greater than room temperature.

3.6. Possible Strategy to Promote OER

From the above discussion, C-doped *p*-BN is predicted as a potential stable photocatalyst for overall water splitting under visible-light. However, it should be noted that the efficiency for OER half-reaction might be not very high because the position of VBM is quite close to the potential of OER (Figure 7, configurations of d, f, and i). It is interesting to ask whether the energy level of VBM could be further modified by carbon doping. Instead of replacing both B and N atoms by C atoms, a *p*-BN model with two B atoms substituted by two C atoms is constructed (**Figure 10**a, configuration of 2B). Surprisingly, as displayed in Figure 10b, the position of VBM for *p*-BN is significantly reduced, which will no doubt greatly enhance the efficiency of OER. Unfortunately, the position of CBM becomes close to the potential of HER, thus resulting in a relatively weak driving force for HER. To the end, a possible strategy of balancing the positions of CBM and VBM is to replace lattice N atom by C atom based on configuration of 2B (Figure 10a, configurations of 2B1N and 2B1N'). As shown in Figure 10b, the VBM and CBM levels of configurations of 2B1N and 2B1N' now match ideally with the potentials of both the OER and HER, suggesting a potential application in photocatalytic overall water splitting with high-performance. This useful strategy might also be applied to engineer the band structures of pristine *h*-BN, even to modify the band structures of graphene-like materials. Further studies will be carried out to support this scenario in the future.

4. Conclusion

In conclusion, the present work adopted first principles computer simulations to demonstrate that C-doped 2D *p*-BN is a potential metal-free photocatalyst for overall water splitting under visible light irradiation. The results showed that carbon doping significantly altered the electronic structures of *p*-BN and obtained a moderate band gap which corresponding to the absorption of visible light. An important finding is that there are no impurity energy levels between the band gaps, thus avoiding the formation of electron-hole recombination center. The calculated

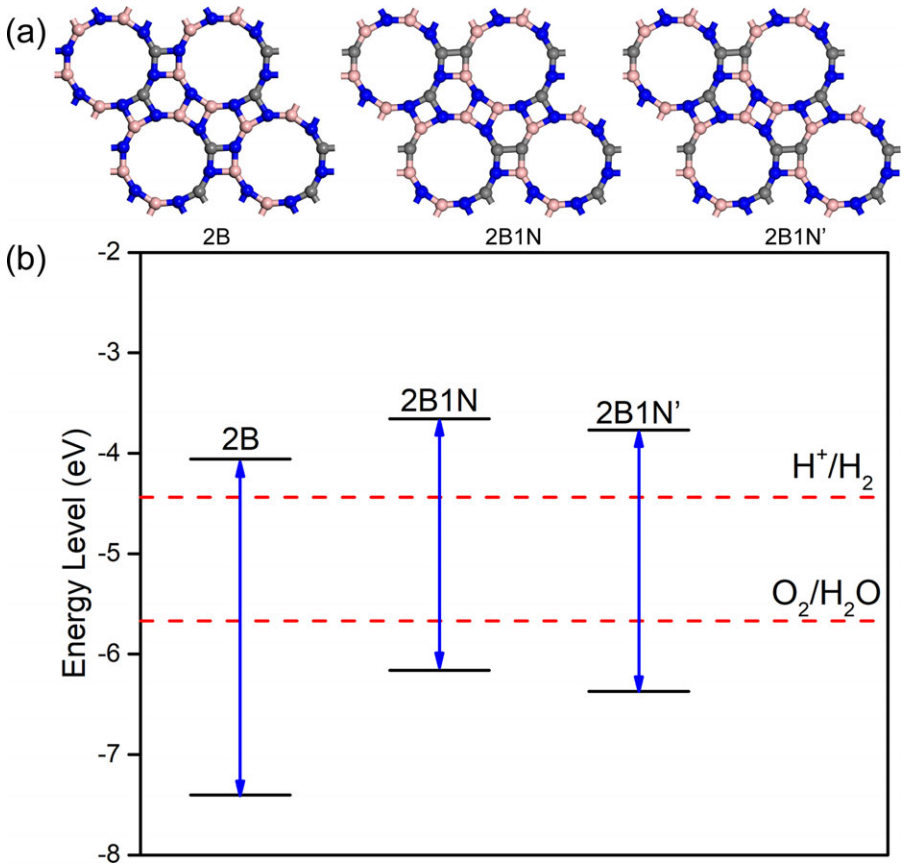

Figure 10. a) Optimized structures of configurations 2B, 2B1N, and 2B1N' with b) the corresponding CBM and VBM. Included are the standard reduction potential of H^+/H_2 (−4.44 eV) and the standard oxidation potential of O_2/H_2O (−5.67 eV) at pH = 0 (relative to the vacuum level).

partial charge density plots corresponding to the VBM and CBM also indicate the photogenerated carriers can be well separated spatially. From the stability testing, it is demonstrated that C-doped *p*-BN structures are very stable, even at high temperatures. More importantly, the VBM and CBM levels of configurations with suitable carbon doping match ideally with the potentials of both the OER and HER, indicating a potential application in photocatalytic overall water splitting. The results from DFT calculations provide a basis to further develop efficient metal-free 2D photocatalysts.

Supporting Information

Supporting Information is available from the Wiley Online Library or from the author.

Acknowledgements

This work was funded by National Natural Science Foundation of China (21673040 to S.L., 21501177 and 21771182 to Z.M.), and Natural Science Foundation of Fujian Province (2016J01052 to S.L.). The authors thank Prof. Xinchen Wang of Fuzhou University and Prof. Hua Guo in University of New Mexico for many useful discussions.

Conflict of Interest

The authors declare no conflict of interest.

Keywords

band structure engineering, metal-free catalysts, overall water splitting, photocatalyst, porous boron nitride nanosheets

Received: November 7, 2018
Revised: December 12, 2018
Published online:

[1] a) K. S. Novoselov, A. K. Geim, S. V. Morozov, D. Jiang, Y. Zhang, S. V. Dubonos, I. V. Grigorieva, A. A. Firsov, *Science* **2004**, *306*, 666; b) K. S. Novoselov, A. K. Geim, S. V. Morozov, D. Jiang, M. I. Katsnelson, I. V. Grigorieva, S. V. Dubonos, A. A. Firsov, *Nature* **2005**, *438*, 197; c) K. S. Novoselov, V. I. Fal'ko, L. Colombo, P. R. Gellert, M. G. Schwab, K. Kim, *Nature* **2012**, *490*, 192.

[2] a) L. Song, L. Ci, H. Lu, P. B. Sorokin, C. Jin, J. Ni, A. G. Kvashnin, D. G. Kvashnin, J. Lou, B. I. Yakobson, P. M. Ajayan, *Nano Lett.* **2010**, *10*, 3209; b) C. Zhi, Y. Bando, C. Tang, H. Kuwahara, D. Golberg, *Adv. Mater.* **2009**, *21*, 2889; c) J. C. Meyer, A. Chuvilin, G. Algara-Siller, J. Biskupek, U. Kaiser, *Nano Lett.* **2009**, *9*, 2683.

[3] a) J. Lu, K. Zhang, X. Feng Liu, H. Zhang, T. Chien Sum, A. H. Castro Neto, K. P. Loh, *Nat. Commun.* **2013**, *4*, 2681; b) Y. Gong, G. Shi, Z. Zhang, W. Zhou, J. Jung, W. Gao, L. Ma, Y. Yang, S. Yang, G. You, R. Vajtai, Q. Xu, A. H. MacDonald, B. I. Yakobson, J. Lou, Z. Liu, P. M. Ajayan, *Nat. Commun.* **2014**, *5*, 3193; c) C. Huang, C. Chen, M. Zhang, L. Lin, X. Ye, S. Lin, M. Antonietti, X. Wang, *Nat. Commun.* **2015**, *6*, 7698.

[4] a) X. Wang, K. Maeda, A. Thomas, K. Takanabe, G. Xin, J. M. Carlsson, K. Domen, M. Antonietti, *Nat. Mater.* **2009**, *8*, 76; b) J. Zhang, G. Zhang, X. Chen, S. Lin, L. Möhlmann, G. Dołęga, G. Lipner, M. Antonietti, S. Blechert, X. Wang, *Angew. Chem. Int. Ed.* **2012**, *51*, 3183.

[5] M. Xu, T. Liang, M. Shi, H. Chen, *Chem. Rev.* **2013**, *113*, 3766.

[6] L. Yin, X. Hai, K. Chang, F. Ichihara, J. Ye, *Small* **2018**, *14*, 1704153.

[7] a) K. Watanabe, T. Taniguchi, H. Kanda, *Nat. Mater.* **2004**, *3*, 404; b) K. K. Kim, A. Hsu, X. Jia, S. M. Kim, Y. Shi, M. Hofmann, D. Nezich, J. F. Rodriguez-Nieva, M. Dresselhaus, T. Palacios, J. Kong, *Nano Lett.* **2012**, *12*, 161; c) Y. Kubota, K. Watanabe, O. Tsuda, T. Taniguchi, *Science* **2007**, *38*, 932.

[8] a) S. N. Shirodkar, U. V. Waghmare, T. S. Fisher, R. Grau-Crespo, *Phys. Chem. Chem. Phys.* **2015**, *17*, 13547; b) R. Quhe, J. Zheng, G. Luo, Q. Liu, R. Qin, J. Zhou, D. Yu, S. Nagase, W.-N. Mei, Z. Gao, J. Lu, *NPG Asia Mater.* **2012**, *4*, e6.

[9] a) Q. Tang, J. Bao, Y. Li, Z. Zhou, Z. Chen, *Nanoscale* **2014**, *6*, 8624; b) Y. Xie, H. Yu, H. Zhang, H. Fu, *Phys. Chem. Chem. Phys.* **2012**, *14*, 4391; c) X. Wang, C. Zhi, L. Li, H. Zeng, C. Li, M. Mitome, D. Golberg, Y. Bando, *Adv. Mater.* **2011**, *23*, 4072; d) Y. Wang, Y. Li, Z. Chen, *J. Phys. Chem. C* **2014**, *118*, 25051.

[10] X. Li, J. Zhao, J. Yang, *Sci. Rep.* **2013**, *3*, 1858.

[11] S. Lin, X. Ye, X. Gao, J. Huang, *J. Mol. Catal. A: Chem.* **2015**, *406*, 137.

[12] a) Y. Ding, Y. Wang, S. Shi, W. Tang, *J. Phys. Chem. C* **2011**, *115*, 5334; b) J. Dai, X. Wu, J. Yang, X. C. Zeng, *J. Phys. Chem. Lett.* **2014**, *5*, 393.

[13] a) C. Gautam, C. S. Tiwary, S. Jose, G. Brunetto, S. Ozden, S. Vinod, P. Raghavan, S. Biradar, D. S. Galvao, P. M. Ajayan, *ACS Nano* **2015**, *9*, 12088; b) J. Xiong, W. Zhu, H. Li, L. Yang, Y. Chao, P. Wu, S. Xun, W. Jiang, M. Zhang, H. Li, *J. Mater. Chem. A* **2015**, *3*, 12738; c) S. Wang, F. Ma, H. Jiang, Y. Shao, Y. Wu, X. Hao, *ACS Appl. Mater. Interfaces* **2018**, *10*, 19588; d) W. Lei, D. Portehault, D. Liu, S. Qin, Y. Chen, *Nat. Commun.* **2013**, *4*, 1777; e) S. M. Gilbert, G. Dunn, A. Azizi, T. Pham, B. Shevitski, E. Dimitrov, S. Liu, S. Aloni, A. Zettl, *Sci. Rep.* **2017**, *7*, 15096.

[14] a) G. Kresse, J. Hafner, *Phys. Rev. B* **1993**, *47*, 558; b) G. Kresse, J. Hafner, *Phys. Rev. B* **1994**, *49*, 14251; c) G. Kresse, J. Furthmüller, *Comput. Mater. Sci.* **1996**, *6*, 15.

[15] a) P. E. Blöchl, *Phys. Rev. B* **1994**, *50*, 17953; b) G. Kresse, D. Joubert, *Phys. Rev. B* **1999**, *59*, 1758.

[16] J. P. Perdew, K. Burke, M. Ernzerhof, *Phys. Rev. Lett.* **1996**, *77*, 3865.

[17] H. L. Zhuang, R. G. Hennig, *Chem. Mater.* **2013**, *25*, 3232.

[18] a) J. Heyd, G. E. Scuseria, M. Ernzerhof, *J. Chem. Phys.* **2003**, *118*, 8207; b) J. Paier, M. Marsman, K. Hummer, G. Kresse, I. C. Gerber, J. G. Angyan, *J. Chem. Phys.* **2006**, *124*, 154709.

[19] a) L. Liu, Y. P. Feng, Z. X. Shen, *Phys. Rev. B* **2003**, *68*, 104102; b) P. Giannozzi, S. de Gironcoli, P. Pavone, S. Baroni, *Phys. Rev. B* **1991**, *43*, 7231; c) A. Nag, K. Raidongia, K. P. S. S. Hembram, R. Datta, U. V. Waghmare, C. N. R. Rao, *ACS Nano* **2010**, *4*, 1539.

[20] a) E. Perim, R. Paupitz, P. A. S. Autreto, D. S. Galvao, *J. Phys. Chem. C* **2014**, *118*, 23670; b) H. Zhang, C.-J. Tong, Y. Zhang, Y.-N. Zhang, L.-M. Liu, *J. Mater. Chem. A* **2015**, *3*, 9632.

[21] a) X. Gonze, C. Lee, *Phys. Rev. B* **1997**, *55*, 10355; b) S. Baroni, S. de Gironcoli, A. Dal Corso, P. Giannozzi, *Rev. Mod. Phys.* **2001**, *73*, 515; c) A. Togo, I. Tanaka, *Scr. Mater.* **2015**, *108*, 1.

[22] a) C.-F. Fu, Q. Luo, X. Li, J. Yang, *J. Mater. Chem. A* **2016**, *4*, 18892; b) Q. Yan, G. Li, P. F. Newhouse, J. Yu, K. A. Persson, J. M. Gregoire, J. B. Neaton, *Adv. Energy Mater.* **2015**, *5*, 1401840.

[23] T. Bak, J. Nowotny, M. Rekas, C. C. Sorrell, *Int. J. Hydrogen Energy* **2002**, *27*, 991.

[24] B. C. Wang, J. Nisar, B. Pathak, T. W. Kang, R. Ahuja, *Appl. Phys. Lett.* **2012**, *100*, 182102.

[25] K. Momma, F. Izumi, *J. Appl. Crystallogr.* **2011**, *44*, 1272.

[26] a) Z. Ma, K. Wu, R. Sa, Q. Li, C. He, Z. Yi, *Int. J. Hydrogen Energy* **2015**, *40*, 980; b) J. Nisar, B. Wang, C. M. Araujo, A. Ferreira da Silva, T. W. Kang, R. Ahuja, *Int. J. Hydrogen Energy* **2012**, *37*, 3014.

[27] a) V. Wang, W. Xiao, D. M. Ma, R. J. Liu, C. M. Yang, *J. Appl. Phys.* **2014**, *115*, 043708; b) G. Tang, Z. Xiao, H. Hosono, T. Kamiya, D. Fang, J. Hong, *J. Phys. Chem. Lett.* **2018**, *9*, 43.

[28] a) V. Chakrapani, J. C. Angus, A. B. Anderson, S. D. Wolter, B. R. Stoner, G. U. Sumanasekera, *Science* **2007**, *318*, 1424; b) S. Trasatti, R. Parsons, *Pure Appl. Chem.* **1986**, *58*, 437.

[29] a) N. Kostoglou, K. Polychronopoulou, C. Rebholz, *Vacuum* **2015**, *112*, 42; b) L. H. Li, J. Cervenka, K. Watanabe, T. Taniguchi, Y. Chen, *ACS Nano* **2014**, *8*, 1457.